Pramana – J. Phys. (2016) 87: 86
DOI 10.1007/s12043-016-1296-5

Parametric study of radiofrequency helium discharge under atmospheric pressure

SAFDAR HUSSAIN*, HAFIZ IMRAN AHMAD QAZI, SHANAWER NIAZ and MANZOOR AHMAD BADAR

Department of Physics, University of Sargodha, 40100 Sargodha, Pakistan
*Corresponding author. E-mail: shussainuos@yahoo.com

MS received 27 July 2015; revised 3 February 2016; accepted 7 March 2016; published online 2 November 2016

Abstract. The parameters of radiofrequency helium discharge under atmospheric pressure were studied by electrical and optical measurements using high voltage probe, current probe and optical emission spectroscopy. Two discharge modes α and γ were observed within certain limits. During α to γ mode transition, a decrease in voltage (280–168 V), current (2.05–1.61 A) and phase angle (76°–56°) occurred. The discharge parameters such as resistance, reactance, sheath thickness, electron density, excitation temperature and gas temperature were assessed by electrical measurements using equivalent circuit model and optical emission spectroscopy. In α mode, the discharge current increased from 1.17 to 2.05 A, electron density increased from 0.19×10^{12} to 0.47×10^{12} cm^{-3} while sheath thickness decreased from 0.40 to 0.25 mm. The excitation temperatures in the α and γ modes were 3266 and 4500 K respectively, evaluated by Boltzmann's plot method. The estimated gas temperature increased from 335 K in the α mode to 485 K in the γ mode, suggesting that the radiofrequency atmospheric pressure helium discharge can be used for surface treatment applications.

Keywords. Atmospheric pressure glow discharge; radiofrequency; excitation temperature; gas temperature.

PACS Nos 52.80.Pi; 52.80.Hc; 52.70.−m; 52.70.Kz

1. Introduction

Atmospheric pressure glow discharge (APGD) plasma represents one of the most exciting research areas in low-temperature plasma physics which has attracted extensive research, largely because it offers a vacuum-less route to many scientific disciplines such as biology, analytical chemistry, medicine, nanoscience, space exploration and display technologies [1–6]. The atmospheric pressure plasmas have outstanding advantages, such as (1) the system is simple and flexible, (2) easy to operate, with no limitations on the size of treated materials and (3) lower capital costs due to the exclusion of expensive and complicated vacuum system, over the widely used low-pressure plasmas [7–13]. APGD plasma sources, because of the former advantages and immense application impact, can be used in a variety of applications such as in surface modification, etching, thin-film deposition, ozone generation, degradation of organic compounds, sterilization, disinfection, biological and chemical decontamination, surface cleaning, food safety and waste treatment [14–21]. Another eye-catching feature of the APGD plasmas is that one can achieve enhanced gas phase chemistry at low gas temperatures. This characteristic opens the horizons for a new era of future plasma technologies, particularly in the emerging field of plasma medicine, allowing treatment of heat sensitive surfaces such as wounds [4,22].

Compared to different types of APGD plasma sources, the radiofrequency (RF) APGD plasmas produced between two naked metallic electrodes have attracted considerable interest of the researchers in recent years, due to the distinct advantage of low breakdown voltage enabling use of smaller power supplies [23–27]. Laimer and Störi [23] investigated the properties of RF APGD plasma generated in helium using bare metallic water-cooled electrodes. They found that sheath breakdown takes place at the maximum current in the α mode and transition to the γ mode occurs which occupies a small portion of the electrode surface. Shi *et al* [24] demonstrated the presence

of normal glow mode and recovery mode in addition to the abnormal glow mode in radiofrequency atmospheric pressure helium glow discharge plasmas. Their electrode system consisted of a grounded metal rod and a powered metal plate with a few millimeters separating them. They reported that sheath breakdown causes mode transition. Li *et al* [25] produced RF APGD plasmas using helium, air, argon, nitrogen or their mixtures as working gas in a planar-type plasma reactor and studied discharge parameters like breakdown voltage, discharge mode and discharge voltage for maintaining the α and γ modes.

The aim of this paper is to describe the properties and obtain the discharge parameters of an atmospheric pressure radiofrequency helium glow discharge by electrical measurements using equivalent circuit model and optical emission spectroscopy.

2. Experimental set-up

The schematic diagram of the experimental set-up and diagnostics is shown in figure 1. The discharge used for this study is produced between two planar square-aluminum electrodes. The effective surface area of each electrode is 20 cm^2 and the spacing between them is fixed at 2.2 mm by using two glass spacers. The top electrode is connected to the RF power supply (Comdel, CX 600AS, 13.56 MHz) via impedance matching network (Match Pro CPM-1000) while the bottom electrode is grounded. The glow discharge is generated by using industrial-grade helium with a flow rate of 3 standard litre per minutes (SLM). Helium is injected from the back side of the electrodes through the teflon mount. After generating glow discharge in the spacing between the electrodes, the working gas is ejected into ambient air. Due to altitude, the average atmospheric pressure of Sargodha is about 992 hPa which is used in the calculation. However, the pressure may change during experiments due to variations in weather condition.

The electrical properties of the discharge are studied by measuring the current and voltage across the discharge simultaneously. The discharge current and the applied voltage are measured by wide-band current (Tektronix P6021 with a bandwidth of 60 MHz) and voltage (Tektronix P5100 with a bandwidth of 250 MHz) probes. The discharge current and applied voltage values and their characteristic waveforms are recorded on a digital oscilloscope (Tektronix TDS 2024B with a sampling rate of 2 G samples/s and a bandwidth of 200 MHz). The electrical data are transferred to a computer. The pictures of the discharge are captured by focussing digital camera (Kodak C 913) through the microscope. The exposure time of the digital camera is 2 ms. Optical emission spectrum is obtained by the spectrometer (Avantes, Avaspec-3648) with charge-coupled device (CCD) detector array and a grating of 1200 grooves/mm and slit width of 10 μm. The wavelength of the spectrometer is calibrated using a mercury lamp before the experiment. More details of this device can be found elsewhere [28].

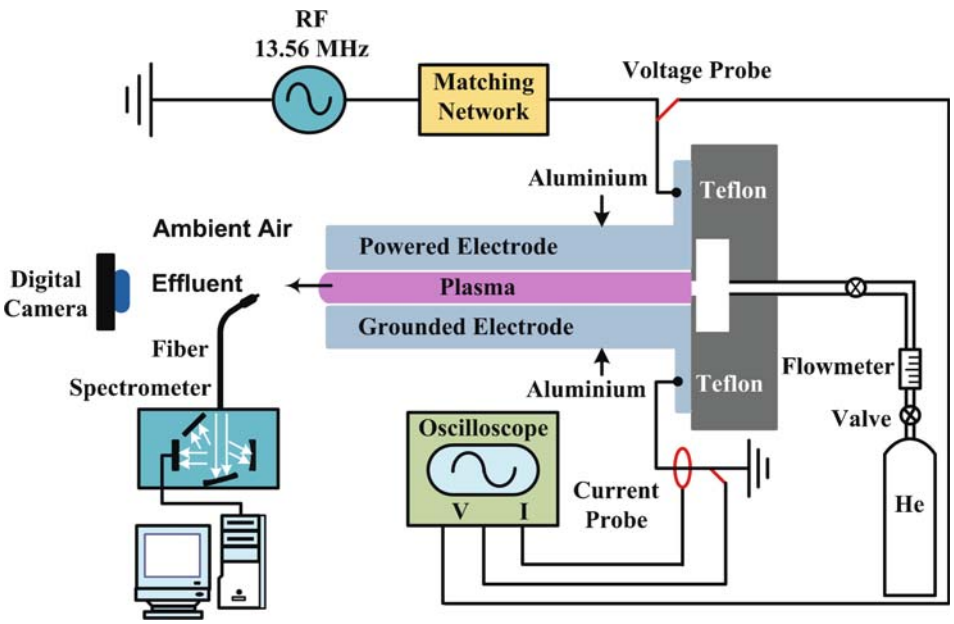

Figure 1. Schematic of the experimental set-up and diagnostics.

3. Results and discussions

The characteristic discharge voltage and current waveforms of the atmospheric helium RF APGD plasma just before and after the mode transition are presented in figure 2. Applied voltage and discharge current traces shown in figure 2 are smooth and mostly sinusoidal, indicating a generally linear response of the discharge. Furthermore, the current waveform leading the voltage waveform, demonstrates that the discharge is capacitive in nature. The phase angle between the current and voltage waveforms just before the mode transition in the α mode and just after the mode transition in the γ mode are 76° and 56°, respectively. The shifts in phase angle of 14° and 34° are due to the resistance arising from the conducting plasma.

Figure 3 shows the voltage–current ($V_{a,r.m.s.}$–$I_{r.m.s.}$) characteristics of the atmospheric helium RF APGD plasma where the root mean square (r.m.s.) values of the applied voltage are plotted as a function of r.m.s. discharge current. In no-discharge regime, discharge current increases linearly with applied voltage and the phase difference between them is 90° indicating purely capacitive impedance. The breakdown occurs at an applied voltage of 185 V. A uniform purplish glow discharge covering only part of the electrodes appears and the phase angle between the current and the voltage decreased from 90° due to the presence of both capacitive and resistive impedances. By increasing the applied voltage, the discharge current increases almost linearly and the $V_{a,r.m.s.}$–$I_{r.m.s.}$ curve has positive differential conductivity suggesting typical abnormal glow mode of the discharge. In this regime, the gradient of the $V_{a,r.m.s.}$–$I_{r.m.s.}$ curve is less than the gradient of the no-discharge regime. At low input powers, partial coverage of the electrodes' surface with glow discharge is observed. As the RF power rises, discharge expands continuously over electrodes until there is full coverage of electrodes' surface with glow discharge. The electrodes become totally covered with glow discharge at a voltage of 212 V and a current of 117 A. Further increase in input power enhances the brightness of the discharge with no change in its size and shape. The glow discharge is volumetric, homogeneous in time and self-sustaining as shown in figure 4a. A comparison of this volumetric discharge with atmospheric helium RF APGD plasma shows that these features are characteristics of the α mode [23,25,27,29].

Upon further increasing the applied voltage to 280 V, an abrupt mode transition occurs. The applied voltage drops from 280 to 168 V, current decreases from 2.05 to 1.61 A and the phase angle reduces from 76° to 56°.

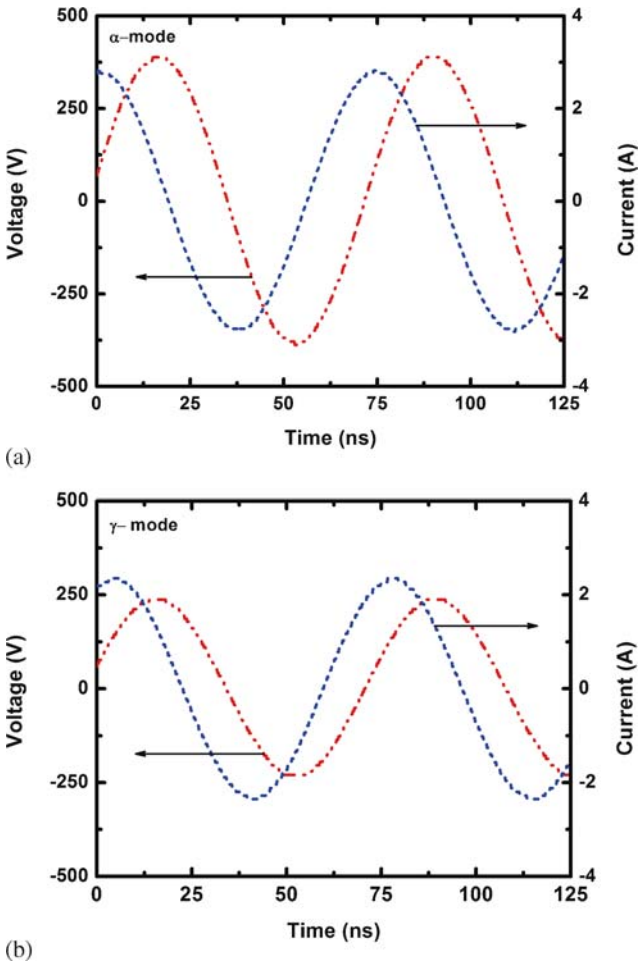

Figure 2. Characteristic traces of the applied voltage and discharge current for helium RF APGD plasma in (**a**) α mode at 2.81 A, 388 V and (**b**) γ mode at 2.35 A, 237 V.

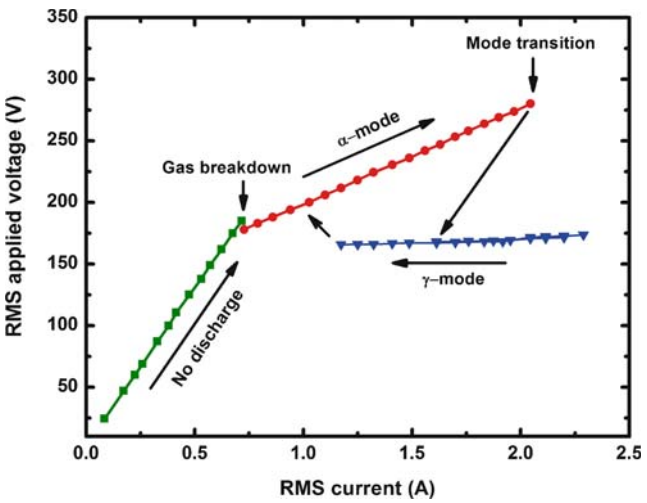

Figure 3. Current–voltage characteristics of helium RF APGD plasma.

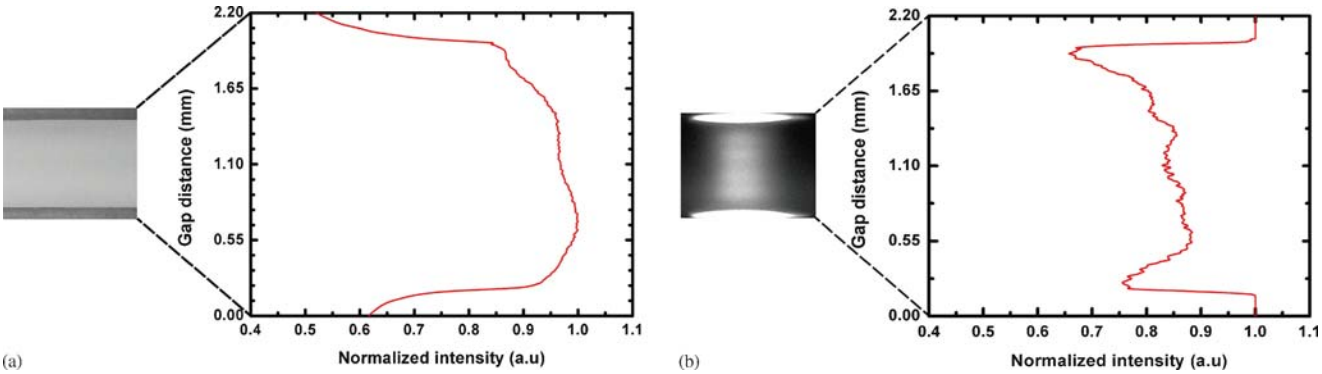

Figure 4. Photograph showing the cross-sectional view of the discharge and the corresponding intensity profile obtained by the image processing of photograph in (**a**) the α mode and (**b**) the γ mode.

The discharge contracts into a less luminous narrow plasma column with intense negative glow near the electrodes. A comparison of this discharge with helium RF APGD plasma shows that these features are characteristic of the γ mode [23,25,27,29]. It is known that in the γ mode, secondary electron emission from the electrodes surface is dominant which enhances the optical emission near the electrodes. This is the reason for the brightest layer to exist near the electrode as shown in figure 4b. By increasing the RF power, current increases and voltage remains fixed at about 168 V. The negative glow as well as the plasma column expands horizontally and a layered structure is observed in a direction normal to the electrodes. Adjacent to each negative glow and in the centre of the gap, the plasma is relatively dim [29]. By decreasing the power, current drops at an almost fixed voltage whereas the size of the negative glow and the number of positive columns are reduced. The γ discharge finally transforms to a pure α discharge. Figure 4 shows magnified photographs of the α and γ discharge modes and the corresponding visible emission intensity profiles obtained by the image processing of the photographs.

To further understand the characteristics of each mode and the transition between them, an equivalent electrical circuit of the RF APGD plasma is required. The RF APGD plasma reactor as a whole is represented by a parallel combination of plasma impedance and parasitic capacitance due to glass spacers etc. [25]. The plasma itself is modelled as a series combination of two capacitors representing the electrode sheaths and a resistor representing the bulk plasma [24,30]. For electrodes (surface area $A = 20$ cm^2) fully covered with glow discharge plasma, the parasitic capacitance (38.3 pF) is calculated by subtracting the capacitance of a parallel plate capacitor (8 pF) from the capacitance measured without a plasma (46.3 pF) evaluated from the slope of no-discharge regime. From the evaluation of measured values of the discharge current, applied voltage and phase angle between them using equivalent circuit model, the discharge resistance and the reactance were obtained. The sheath thickness can be determined using the equation [31]

$$d_s = 0.76\,\varepsilon_0(2\pi f)XA, \tag{1}$$

where ε_0 is the permittivity of free space (Fm^{-1}), $f = 13.56$ MHz in this case, X is the discharge reactance and A is the discharge area (m^2).

The electron number density of the bulk plasma can be calculated using the equation [25,26]

$$j = -en_e\mu_e E, \tag{2}$$

where j is the current density of the plasma bulk, e is the unit charge, μ_e is the electron mobility ($\mu_e P = 0.86 \times 10^6$ cm^2 Torr/V s) for helium [30] and E is the electric field of the bulk plasma which is calculated using the equation [25]

$$E = \frac{jRA}{(d - 2d_s)}, \tag{3}$$

where R is the resistance of the bulk plasma and d is the gap spacing.

From the formulas given above, the resistance, reactance, sheath thickness and electron number density were calculated in the current range 1.17–2.05 A. The results of calculations for full coverage of electrodes with helium α discharge are shown in figure 5. Figure 5a presents the variation of resistance, reactance and their ratio with discharge current in the α mode. Both resistance and reactance decrease with increase in discharge current. In this case, the rise in input power is used to increase ionization in the fixed plasma area which increases the discharge current and

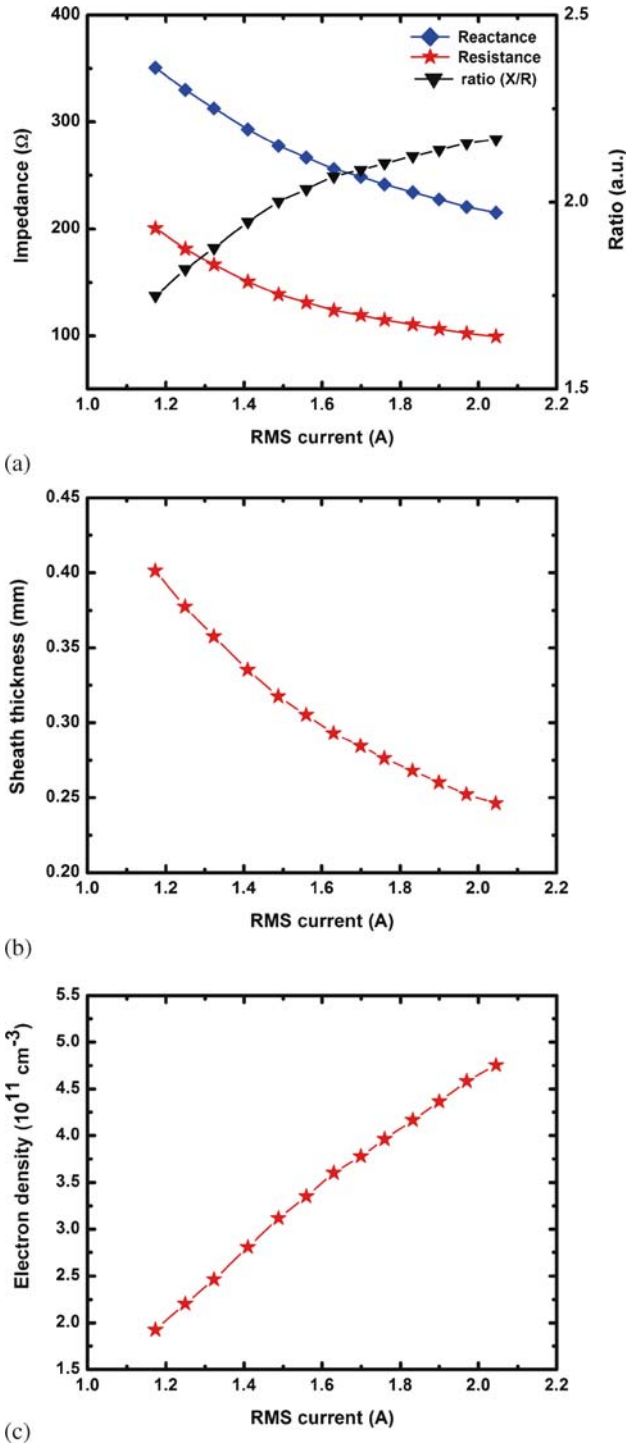

Figure 5. Variation of (**a**) discharge resistance, reactance and their ratio, (**b**) sheath thickness and (**c**) electron number density, with discharge current for fully covered electrodes with α discharge.

the current density. Increase in ionization decreases the discharge resistance and increases the capacitance due to the decrease of sheath thickness as is evident from figure 5b. However, increase in the ratio X/R in figure 5a indicates that the increase in capacitance was smaller than the decrease in resistance.

Figure 5b presents the sheath thickness as a function of discharge current. Note that the helium sheath thickness decreases monotonically from 0.40 to 0.25 mm as the discharge current increases from 1.17 to 2.05 A. Laimer and Störi [23] calculated sheath thickness as 0.34 mm for atmospheric pressure contaminated helium glow discharge just before α to γ mode transition with 2.5 mm spacing between the electrodes. Park *et al* [32] estimated sheath thickness for atmospheric pressure high-purity helium at 1.6 mm spacing from spatial profiles of emission intensity and obtained a value of 0.35 mm, while Moon *et al* [27] calculated sheath thickness as 0.5 mm using visible emission intensity profiles and simple series circuit model.

The electron number density vs. discharge current is plotted in figure 5c. The electron density increases from 0.19×10^{12} to 0.47×10^{12} cm^{-3} as the discharge current increases from 1.17 to 2.05 A. Park *et al* [33] obtained the electron density as 0.29×10^{12} cm^{-3} from neutral bremsstrahlung measurements for atmospheric pressure contaminated helium glow discharge at 2.4 mm spacing. Moravej *et al* [26] determined the electron density as 0.93×10^{12} cm^{-3} for atmospheric pressure high purity helium glow discharge at 1.6 mm spacing between electrodes. Laimer and Störi [23] calculated the electron density as 0.22×10^{12} cm^{-3} just before α to γ mode transition with contaminated helium at atmospheric pressure for 2.5 mm spacing. Therefore, electron number density and sheath thickness for α discharge of helium exhibited in figure 5 almost match the corresponding values presented in [23,26,32,33].

Figures 6a and 6b present the visible emission spectra in 300–800 nm wavelength range recorded at 2.05 and 1.61 A r.m.s. discharge currents corresponding to the α and γ modes, respectively. The excited helium atomic lines 388.9, 447.2, 471.3, 492.1, 501.5, 587.5, 667.8, 706.5 and 728.1 nm are dominantly observed because helium is the working gas. In addition, OH line at 309 nm, excited N_2 lines at 337 nm and 357 nm, N_2^+ line at 391.4, H_α line at 656.6 nm and atomic oxygen line at 777 nm can clearly be seen in figure 6. Nitrogen, oxygen and OH lines appear due to the plasma forming in ambient air and the impurities in the industrial grade helium. The emission intensity of the entire spectral range in the γ mode is significantly more than that in the α mode.

In this study, excitation temperature which provides information about the concentration of plasma's species was measured by Boltzmann's plot method [34]. The excitation temperature is determined using

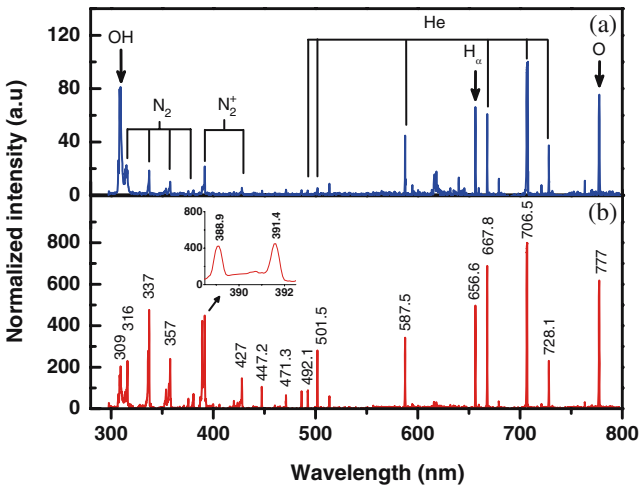

Figure 6. Optical emission spectra of He APGD plasma in (**a**) α mode at $I_{\text{r.m.s.}} = 2.05$ A and (**b**) γ mode at $I_{\text{r.m.s.}} = 1.61$ A.

intensities of several spectral lines, assuming that the population of the emitting levels obeys the Boltzmann's distribution [35]. The excitation temperature is obtained from the following equation:

$$\ln\left(\frac{I_{ki}\lambda_{ki}}{g_k A_{ki}}\right) = -\frac{E_k}{k_B T_{\text{exc}}} + C, \tag{4}$$

where λ_{ki} is the wavelength, I_{ki} is the measured intensity, A_{ki} is the transition probability, g_k is the statistical weight of the upper level, k_B is the Boltzmann constant and T_{exc} is the excitation temperature. With the help of the calibrated spectroscopic set-up, the following He–I spectral lines at 471.3, 492.1, 587.5, 667.8, 706.5 and 728.1 nm are obtained and used for the Boltzmann's plot [36]. Table 1 presents the data for the selected He–I spectral lines [37].

In figures 7a and 7b, the function $\ln(I\lambda/gA)$ vs. the energy of the upper level is plotted for each transition considered and the excitation temperature in the α and γ modes is obtained from the slope using eq. (4). The excitation temperature increases from 3266 K in the α mode to 4500 K in the γ mode. The intensity of helium atomic lines emitted from levels having energy

Table 1. Helium spectral lines used for the excitation temperature measurements [37].

Transition	λ (nm)	A_{ki} (10^8 s^{-1})	g_k	E (eV)
$4^3S \rightarrow 2^3P$	471.3	0.0528	3	23.59
$4^1D \rightarrow 2^1P$	492.1	0.198	5	23.73
$3^3D \rightarrow 2^3P$	587.5	0.294	3	23.07
$3^1D \rightarrow 2^1P$	667.8	0.637	5	23.07
$3^3S \rightarrow 2^3P$	706.5	0.0309	3	22.71
$3^1S \rightarrow 2^1P$	728.1	0.182	1	22.92

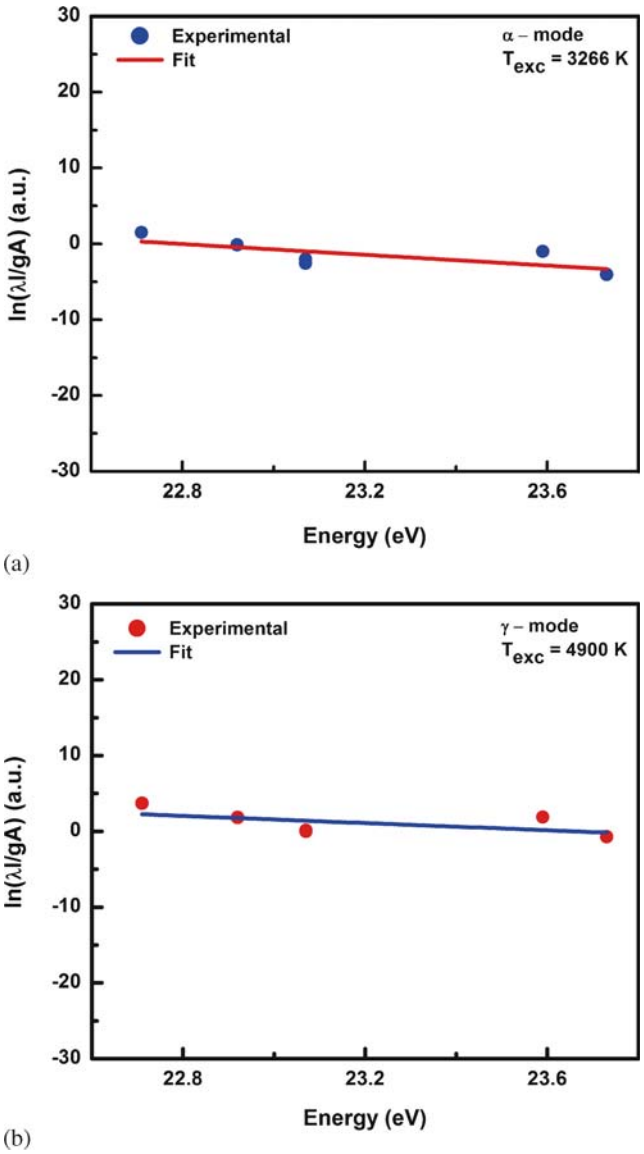

Figure 7. Boltzmann's plot of the selected He-I spectral lines for (**a**) α and (**b**) γ modes. The excitation temperatures obtained from Boltzmann's plot are 3266 K for the α mode and 4900 K for the γ mode.

close to the helium ionization energy 24.58 eV, such as 471.3 and 492.1 nm, increases in the γ mode due to the increase in excitation temperature from 3266 K in the α mode to 4500 K in the γ mode. A comparison of the results shows that the excitation temperature of the He RF APGD plasma tallies with the other He RF atmospheric plasmas [27]. However, it is lower than that of low-pressure He glow discharges [34]. At atmospheric pressure, the electron-neutral collision frequency is huge as a result of small order of mean free paths. That is why the electrons are able to accumulate very small amount of energy leading to low excitation

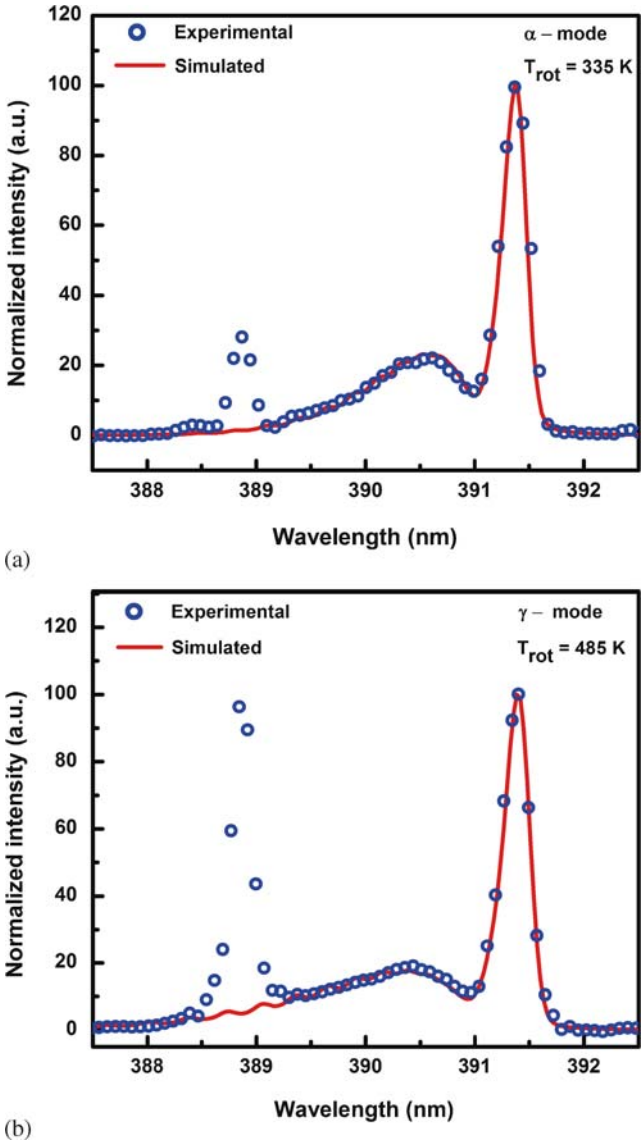

Figure 8. The comparison of the measured N_2^+ molecular spectrum with LIFBASS-generated synthetic spectrum. The estimated rotational temperatures for the α mode and the γ mode are 335 K and 485 K, respectively.

temperatures as compared to low-pressure helium glow discharges.

At atmospheric pressure, the gas temperature can be deduced from rotational temperature due to the frequent collisions among heavy particles [38]. The optical emission spectrum of N_2^+ molecular band is used to estimate the gas temperature. The gas temperature is obtained by comparing the shape of the synthetic spectrum generated by LIFBASS with the measured N_2^+ line around 391.4 nm [39]. This program assumes that the rotational states are Boltzmann-distributed. The best fit between the experiment and the simulation reveals the rotational temperature of the experiment. Typical fitting of the measured spectrum with synthetic spectrum in the α and γ mode are shown in figures 8a and 8b. The simulated spectra at 335 K and 485 K rotational temperatures give best fit to the measured spectra in the α and γ modes, respectively. Therefore, the gas temperature of He RF APGD plasma is 335 K in the α mode and 485 K in the γ mode. This gas temperature is suitable for surface modification applications [14].

4. Conclusions

In a nutshell, the helium RF APGD plasma exhibited α and γ operation modes. The discharge parameters such as resistance, reactance, sheath voltage, sheath thickness, electron number density, excitation temperature and gas temperature were obtained by electrical measurements using equivalent circuit model and optical emission spectroscopy. The assessed values were within a reasonable range. The excitation temperature increased from 3266 K in the α mode to 4500 K in the γ mode. The estimated gas temperature increased from 335 K in the α mode to 485 K in the γ mode, suggesting that the radiofrequency atmospheric pressure helium discharge can be used for surface treatment of materials.

Acknowledgement

This work is partially supported by the Higher Education Commission Project No. 1852.

References

[1] H B Wang, W T Sun, H P Li, C Y Bao, X Gao and H Y Luo, *Appl. Phys. Lett.* **89**, 161504 (2006)
[2] S Hussain, H I A Qazi and M A Badar, *Phys. Plasmas* **21**, 030702 (2014)
[3] H Shirai, Y Kobayashi and T Hasegawa, *Appl. Phys. Lett.* **87**, 143112 (2005)
[4] D B Graves, *Phys. Plasmas* **21**, 080901 (2014)
[5] A Fruchtman, *Phys. Rev. Lett.* **96**, 065002 (2006)
[6] H S Uhm, C G Son, B H Hong and E H Choi, *Phys. Plasmas* **16**, 094503 (2009)
[7] S Sharma and M M Turner, *Phys. Plasmas* **20**, 073507 (2013)
[8] M A Lieberman, *IEEE Trans. Plasma Sci.* **16**, 638 (1988)
[9] S Sharma and M M Turner, *Plasma Sources Sci. Technol.* **22**, 035014 (2013)
[10] M M Turner, *Phys. Rev. Lett.* **75**, 1312 (1995)
[11] I D Kaganovich, *Phys. Rev. Lett.* **89**, 265006 (2002)
[12] S Sharma, S K Mishra and P K Kaw, *Phys. Plasmas* **21**, 073511 (2014)
[13] S Sharma, S K Mishra, P K Kaw, A Das, N Sirse and M M Turner, *Plasma Sources Sci. Technol.* **24**, 025037 (2015)
[14] S Y Moon, J W Han and W Choe, *Thin Solid Films* **506–507**, 355 (2006)

[15] Q Y Nie, H I A Qazi, H P Li, J Y Chen and C Y Bao, *IEEE Trans. Plasma Sci.* **42**, 2628 (2014)
[16] M Sato, *Plasma Sources Sci. Technol.* **17**, 024021 (2008)
[17] X Hua, J Wang, Z Wu, H Zhang, H P Li, X Xing and Z Liu, *Biochem. Eng. J.* **49**, 201 (2010)
[18] S Ono, S Teii, Y Suzuki and T Suganuma, *Thin Solid Films* **518**, 981 (2009)
[19] G Li, H P Li, L Y Wang, S Wang, H X Zhao, W T Sun, X H Xing and C Y Bao, *Appl. Phys. Lett.* **92**, 221504 (2008)
[20] H W Herrmann, I Henins, J Park and G S Selwyn, *Phys. Plasmas* **6**, 2284 (1999)
[21] M Vleugels, G Shama, X T Deng, E Greenacre, T Brocklehurst and M G Kong, *IEEE Trans. Plasma Sci.* **33**, 824 (2005)
[22] M Keidar, A Shashurin, O Volotskova, M A Stepp, P Srinivasan, A Sandler and B Trink, *Phys. Plasmas* **20**, 057101 (2013)
[23] J Laimer and H Störi, *Plasma Process. Polym.* **3**, 573 (2006)
[24] J J Shi, X T Deng, R Hall, J D Punnett and M G Kong, *J. Appl. Phys.* **94**, 6303 (2003)
[25] H P Li, W T Sun, H B Wang, G Li and C Y Bao, *Plasma Chem. Plasma Process.* **27**, 529 (2007)
[26] M Moravej, X Yang, G R Nowling, J P Chang, R F Hicks and S E Babayan, *J. Appl. Phys.* **96**, 7011 (2004)
[27] S Y Moon, J K Rhee, D B Kim and W Choe, *Phys. Plasmas* **13**, 033502 (2006)
[28] H I A Qazi, M Sharif, S Hussain, M A Badar and H Afzal, *Plasma Sci. Technol.* **15**, 900 (2013)
[29] S Hussain, H I A Qazi, A A Malik and M A Badar, *IEEE Trans. Plasma Sci.* **42**, 2410 (2014)
[30] Y P Raizer, M N Shneider and N A Yatsenko, *Radio-frequency capacitive discharge* (CRC Press, Boca Raton, 1995)
[31] M A Lieberman and A J Lichtenberg, *Principles of plasma discharges and materials processing* (Wiley, New York, 1994)
[32] J Park, I Henins, H W Herrmann, G S Selwyn and R F Hicks, *J. Appl. Phys.* **89**, 20 (2001)
[33] J Park, I Henins, H W Herrmann, G S Selwyn and R F Hicks, *Phys. Plasmas* **7**, 3141 (2000)
[34] M A Naveed, A Qayyum, A Shujaat and M Zakaullah, *Phys. Lett. A* **359**, 499 (2006)
[35] C Biloiu, H Ehrich and G Musa, *J. Vac. Sci. Technol. A* **19**, 757 (2001)
[36] W L Wiese, M W Smith and B M Glennon, *Atomic transition probabilities* (NSRDS, Washington DC, 1966)
[37] http://physics.nist.gov/cgi-bin/ASD
[38] G Herzberg, *Molecular spectra and molecular structure: 1. Spectra of diatomic molecules* (Van Nostrand Company, Princeton, 1964)
[39] J Luque and D R Crosley, SRI International Report No. MP 99-009 (1999), http://www.sri.com/psd/lifbase